Precession of the lunar core

Citation: Meyer, Jennifer, and Jack Wisdom. "Precession of the Lunar Core." Icarus 211, no. 1 (January 2011): 921–924.

As Published: http://dx.doi.org/10.1016/j.icarus.2010.09.016

Publisher: Elsevier

Persistent URL: http://hdl.handle.net/1721.1/103937

Version: Author's final manuscript: final author's manuscript post peer review, without publisher's formatting or copy editing

Precession of the Lunar Core

Jennifer Meyer and Jack Wisdom

Massachusetts Institute of Technology, Cambridge, MA 02139

meyerj@mit.edu, wisdom@mit.edu

Manuscript pages: 11
Figures: 3
Tables: 0

Running head: Precession of the Lunar Core

Corresponding author:

Jennifer Meyer
54-410 MIT
Cambridge, MA 02139

Abstract:

Goldreich (1967) showed that a lunar core of low viscosity would not precess with the mantle. We show that this is also the case for much of lunar history. But when the Moon was close to the Earth the Moon's core was forced to follow closely the precessing mantle, in that the rotation axis of the core remained nearly aligned with the symmetry axis of the mantle. The transition from locked to unlocked core precession occurred between 26.0 and 29.0 Earth radii, thus it is likely that the lunar core did not follow the mantle during the Cassini transition. Dwyer and Stevenson (2005) suggested that the lunar dynamo needs mechanical stirring to power it. The stirring is caused by the lack of locked precession of the lunar core. So, we do not expect a lunar dynamo powered by mechanical stirring when the Moon was closer to the Earth than 26.0 to 29.0 Earth radii. A lunar dynamo powered by mechanical stirring might have been strongest near the Cassini transition.

Key words: Moon; Interiors; Rotational dynamics; Satellites, dynamics

1. Introduction

Paleomagnetic measurements of lunar rocks show magnetic remanence most easily explained by a long-lived early lunar dynamo (Garrick-Bethell et al. 2009). Dwyer and Stevenson (2005) argued that the only plausible driving force for an early lunar dynamo is mechanical stirring of the liquid core due to the relative motion between the core and mantle. This driving mechanism is only an option if the core of the Moon does not precess along with the mantle.

The orbit of the Moon is inclined by about 5 degrees to the ecliptic and regresses with an 18.6 year period. The rotation of the Moon is synchronous with the orbital motion. The spin axis of the solid Moon is tilted with respect to the ecliptic and its precession is locked to the precession of the orbit: the Moon is in a Cassini state (Peale 1968). Goldreich (1967) showed that a liquid lunar core of low viscosity would not precess with the mantle; the spin axis of the lunar core is nearly normal to the ecliptic. For the Earth, the core precesses with the mantle because of the inertial coupling mechanism (Poincaré 1910; Toomre 1966). That is, the spin axis of the Earth's fluid core is nearly parallel to the spin axis of the mantle, and both regress with a period of roughly 26,000 years. Goldreich showed that the inertial coupling mechanism fails for the Moon, arguing that the ellipticity of the core-mantle boundary is smaller than required to cause the core to precess with the mantle. We address here whether the lunar core precessed with the mantle at earlier epochs.

If the core is locked to the mantle (as for the Earth), then the spin axis of the core is nearly aligned with the symmetry axis of the core-mantle boundary. If the spin axis of the core is slightly displaced from this configuration then the spin axis precesses about the symmetry axis with the core precession frequency ω_c (Touma and Wisdom 2001)

$$\omega_c = \omega \, f_c \, (C/C_m), \tag{1}$$

where ω is the rotation frequency of the Moon, f_c is the core flattening, and C/C_m, the ratio of the polar moment of inertia of the Moon to that of the mantle (the Moon excluding the core), is approximately 1 for the Moon. The core flattening is given by $f_c = (C_c - A_c)/C_c$ where A_c and C_c are the smallest and largest moments of inertia of the core. If the core is not locked to the mantle, then the spin axis is no longer closely aligned with the core-mantle boundary symmetry axis.

Whether the core is locked to the mantle depends on the relative frequencies of the precession of the core and the mantle (Poincaré 1910). If the mantle precesses faster than the core $\omega_m > \omega_c$, as is the case today, the core will not follow the mantle. However, if the precession frequency of the core is larger than that of the mantle $\omega_c > \omega_m$, the core and mantle will precess together, with the core oscillating around the symmetry axis of the mantle with the frequency ω_c. Since C/C_m is approximately unity, we may restate the condition for locking in terms of the flattening. Locking occurs for core flattening larger than ω_m/ω. In the limit of very small flattening, the rotation axis of the core is perpendicular to the ecliptic plane.

Goldreich argued that the lunar core flattening is too small today for the inertial coupling mechanism to lock the core to the mantle. But earlier in the lunar history, the Moon was closer to the Earth, and rotated more rapidly, so the Moon was subject to greater tidal and centrifugal forces. Thus the lunar core flattening was larger in the past.

Here, we model the past ellipticity of the lunar core-mantle boundary and compare the estimated precession rate of the core to that of the mantle to determine when the lunar core was locked to the mantle.

2. Model and Results

We assume that the Moon rotates synchronously with its orbital motion. We take the orbit of the Moon to be circular, as the effect of eccentricity on the precession of the Moon is small (Touma and Wisdom 1994). The Moon's orbit is inclined and precessing. For the history of the lunar orbit under these assumptions we use the model of Touma and Wisdom (1994). They examined various tidal models and found that the basic evolution did not depend on the tidal model. Here we use the Mignard model from that work. We approximate the density in the Moon by a two layer model, with constant density in the mantle and in the core. The core is presumed to be fluid.

The surface and core-mantle boundary are out of round: we describe these surfaces by the shape functions

$$r_i(\theta, \phi) = a_i(1 + \epsilon^i_{20} P_2(\cos\theta) + \epsilon^i_{22} P_{22}(\cos\theta)\cos(2\phi)), \tag{2}$$

where $P_2(x) = (3x^2 - 1)/2$ and $P_{22}(x) = 3(1 - x^2)$, and θ is the colatitude, ϕ is the longitude measured from the sub-Earth point, and a_i is the mean radius. The shape function r_i gives the radius of the surface as a function of colatitude and longitude. The label i is either "c" for core or "s" for surface. We can relate the flattening to the shape parameter $f_c = -(3/2)\epsilon^c_{20}$. This was derived by performing the integrals for the principal moments.

The origin of the low order shape and moments of the Moon is still discussed. The "fossil bulge" hypothesis asserts that the shape was determined at an early epoch and has been constant since that epoch. Explaining that shape has been difficult however; one possibility is that the shape formed when the Moon was in a moderately eccentric orbit (Garrick-Bethell et al. 2006), though Meyer and Wisdom (2010) argue against this scenario. We adopt the fossil bulge hypothesis, though it is unclear at what time (what lunar semimajor axis) the fossil bulge was established. At earlier epochs we presume the shape of the mantle of the Moon was approximately hydrostatic.

We consider two simplified models. In one model, the "non-hydrostatic mantle" model, we consider the shape of the mantle (its surface) to be responsible for the low order moments of the Moon, and find the shape of the core-mantle boundary by assuming its shape is hydrostatic, i.e. that the total potential is constant on that surface. In the other model, the "hydrostatic mantle" model, we determine both the shape of the surface and the shape of the core-mantle boundary by assuming they are both hydrostatic. We expect the hydrostatic model to be applicable early in the lunar evolution, and the non-hydrostatic model to be applicable later (presuming the fossil bulge hypothesis), though the point of transition is unclear.

The potential acting on a particular mass element in the Moon with radius r, colatitude θ, and longitude ϕ is given by

$$U = U_{rot} + U_{tidal} + U_m, \tag{3}$$

where the rotational (centrifugal) potential is

$$U_{rot} = \frac{1}{3}\omega^2 r^2 P_2(\cos\theta), \tag{4}$$

the tidal potential is

$$U_{tidal} = -\frac{GMr^2}{r_p^3} P_2(\cos\alpha), \tag{5}$$

and U_m is the potential due to the mass distribution in the Moon, and where α is the angle of the mass element from the Earth-Moon line measured from the center of the Moon, ω is the rotational/orbital frequency of the Moon, G is the gravitational constant, M is the mass of the Earth, and $r_p = a$ is the semimajor axis of the Moon (not to be confused with a_c and a_s).

For a synchronous Moon with zero obliquity in a circular orbit, the angle α is given by $\cos\alpha = \sin\theta\cos\phi$. But the Moon has a small non-zero inclination and obliquity. The tidal potential thus has periodic variations, on an orbital period. The average tidal potential governs the shape, because variations in hydrostatic shape occur on a timescale long compared to the variations in the tidal potential. The average tidal potential differs from that for zero obliquity by terms of second order in the small obliquity. For most of the history of the lunar orbit, these periodic variations in the tidal potential are ignorable. An exception occurs during the Cassini transition, which occurs near $33.4R_e$ (Ward 1975; Wisdom 2006), during which the Moon briefly develops large obliquity. Taking account of obliquity, the average tidal potential is

$$\begin{aligned} U_{tidal} &= -\frac{GMr^2}{r_p^3}\left[P_{20}(\cos\theta)\left(-\frac{1}{2}+\frac{3}{4}(\sin\varepsilon)^2\right)\right. \\ &\qquad \left. P_{22}(\cos\theta)\cos(2\phi)\left(\frac{1}{4}-\frac{1}{16}(\sin(\varepsilon))^2-\frac{1}{4}\left(\sin(\varepsilon/2)\right)^2\right)\right], \end{aligned} \tag{6}$$

where ε is the obliquity of the spin axis to the orbit. This can be derived by first computing $\cos\alpha$ for an arbitrary point in the synchronously rotating but oblique Moon. Then form the potential, average it over time, and reexpress the position in terms of the Legendre polynomials. For the obliquity as a function of semimajor axis we use the results of Wisdom (2006).

For a homogeneous body (uniform density ρ_m) with surface shape function r_s, mean radius a_s, and parameters ϵ^s_{20} and ϵ^s_{22}, the exterior potential is (Jefferys, 1976)

$$U^s_{ext}(r,\theta,\phi) = -\frac{4}{3}\pi G\rho a_s^3\left(\frac{1}{r}+\frac{3}{5}\frac{a_s^2}{r^3}\epsilon^s_{20}P_2(\cos\theta)+\frac{3}{5}\frac{a_s^2}{r^3}\epsilon^s_{22}P_{22}(\cos\theta)\cos(2\phi)\right), \tag{7}$$

and the interior potential is

$$U^s_{int}(r,\theta,\phi) = -\frac{4}{3}\pi G\rho a_s^3\left(\frac{3a_s^2-r^2}{2a^3}+\frac{3}{5}\frac{r^2}{a_s^3}\epsilon^s_{20}P_2(\cos\theta)+\frac{3}{5}\frac{r^2}{a_s^3}\epsilon^s_{22}P_{22}(\cos\theta)\cos(2\phi)\right), \tag{8}$$

These expressions are correct to first order in the shape parameters. Note that at the radius $r = a_s$ the exterior potential and the interior potential agree to first order in the shape parameters, so at this order we can use the two potentials interchangably.

For a body that has, in addition, an out-of-round core, we add to this potential the potential due to a core of additional density $\Delta\rho = \rho_c - \rho_m$. The additional potential exterior to the core-mantle boundary is

$$U^c_{ext}(r,\theta,\phi) = -\frac{4}{3}\pi G\,\Delta\rho\,a_c^3\left(\frac{1}{r} + \frac{3}{5}\frac{a_c^2}{r^3}\epsilon^c_{20}P_2(\cos\theta) + \frac{3}{5}\frac{a_c^2}{r^3}\epsilon^c_{22}P_{22}(\cos\theta)\cos(2\phi)\right), \quad (9)$$

and the additional potential interior to the core-mantle boundary is

$$U^c_{int}(r,\theta,\phi) = -\frac{4}{3}\pi G\,\Delta\rho\,a_c^3\left(\frac{3a_c^2 - r^2}{2a^3} + \frac{3}{5}\frac{r^2}{a_c^3}\epsilon^c_{20}P_2(\cos\theta) + \frac{3}{5}\frac{r^2}{a_c^3}\epsilon^c_{22}P_{22}(\cos\theta)\cos(2\phi)\right). \quad (10)$$

The potential U_m at the core-mantle boundary is

$$U_m^{cmb}(\theta,\phi) = U^s_{int}(r_c(\theta,\phi),\theta,\phi) + U^c_{ext}(r_c(\theta,\phi),\theta,\phi), \quad (11)$$

and the potential U_m at the surface is

$$U_m^{surf}(\theta,\phi) = U^s_{ext}(r_s(\theta,\phi),\theta,\phi) + U^c_{ext}(r_s(\theta,\phi),\theta,\phi). \quad (12)$$

The total potential on these surfaces in addition includes the rotational and tidal contributions.

We solve two problems: (1) given the shape parameters for the mantle determined by matching the observed gravitational moments, find the hydrostatic shape of the core-mantle boundary (we call this the "non-hydrostatic mantle" case), and (2) find the hydrostatic shape of both the mantle and the core (we call this the "hydrostatic mantle" case). We solve both models as a function of the Earth-Moon distance (semimajor axis of the assumed circular orbit).

We use two methods of solution. In one method we define a function that is nonzero and positive if the surfaces that should be hydrostatic are non-hydrostatic. This function takes a number of differences of the potential at different colatitudes and longitudes, squares them, and sums over all differences taken. We then find the shape parameters by minimizing

this function over the shape parameters, using the Nelder-Mead downhill simplex method. In the second method, we truncate the potentials at first order in the shape parameters. We then project the potentials (which are functions of colatitude and longitude) onto the second degree spherical harmonics, $P_2(\cos\theta)$ and $P_{22}(\cos\theta)\cos(2\phi)$, by performing the integrals of the products of these functions, the total potential on each surface, and the surface area element. The result is a set of linear equations in the shape parameters that we solved analytically, but are too complicated to display. The shape parameters determined by the two methods agree to first order in the shape parameters, about four or five digits.

Williams et al. (2009) found that the ratio of the core moment to the total moment of inertia of the Moon C_c/C was $1.2 \pm 0.4 \times 10^{-3}$. In Figure 1, we show the core flattening calculated for the hydrostatic and non-hydrostatic mantle models as a function of the core density, for three values of C_c/C. We vary the core density from 4700 kg/m^3 (Fe-FeS eutectic) to 8100 kg/m^3 (pure Fe) (Kuskov and Kronrod 1998). The flattening is not sensitive to the assumed C_c/C as demonstrated in the figure (though the radius of the core does depend on the assumed C_c/C).

For the non-hydrostatic mantle model we use

$$C_{20} = \frac{(B+A)/2 - C}{ma_e^2} = -2.04 \times 10^{-4} \tag{13}$$

and

$$C_{22} = \frac{B-A}{4ma_e^2} = 2.24 \times 10^{-5}, \tag{14}$$

determined from the libration parameters (Dickey et al. 1994). These correspond to mantle shape parameters of $\epsilon^s_{20} = -3.40 \times 10^{-4}$ and $\epsilon^s_{22} = 3.74 \times 10^{-5}$, ignoring small contributions from the core. Here m is the mass of the Moon, and a_e is the mean equatorial radius. The principal moments of the Moon are $A < B < C$.

There is marginal detection of the ellipticity of the lunar core-mantle boundary from laser ranging analysis (Williams et al. 2009). They find the flattening of the core-mantle boundary to be $f_c = 2.0 \pm 2.3 \times 10^{-4}$. The large error bar is argued to be more a reflection of a correlation in the result with other uncertain parameters rather than uncertainty in the flattening. Williams et al. (2009) notes that the core flattening is not hydrostatic (by comparing the result to the expected hydrostatic core-mantle boundary with a hydrostatic

mantle). Of course, the fact that the mantle is currently non-hydrostatic is well known. We can see from Figure 1 that the observed flattening agrees well with the hydrostatic flattening expected of the core-mantle boundary inside a non-hydrostatic mantle (the non-hydrostatic mantle model).

Emboldened by this success, we now calculate the hydrostatic flattening of the core-mantle boundary as the lunar orbit evolves. Figure 2 shows the results. The parameters we adopt are: $a_c = 350$km, $a_s = 1738$km, $\Delta\rho = 4400\text{kg/m}^3$, $\rho = 3300\text{kg/m}^3$. For the present lunar orbit we find, in the hydrostatic mantle case, $\epsilon^c_{20} = -1.01 \times 10^{-5}$; and, for the non-hydrostatic mantle case, we find $\epsilon^c_{20} = -1.39 \times 10^{-4}$. These correspond to core flattening parameters of $f_c = 1.52 \times 10^{-5}$ and $f_c = 2.09 \times 10^{-4}$. We see that at large semimajor axes the precession of the fluid core is not coupled to the precession of the mantle, but at small semimajor axes the two precess together. The point of transition is uncertain ($26.0R_e$ - $29.0R_e$, where R_e is the radius of the Earth), because the semimajor axis at which the Moon developed its nonhydrostatic shape is uncertain. The time is much more uncertain, as the timescale for tidal evolution early in the lunar history is unknown. But assuming average tidal parameters such that the orbit of the Moon reaches the Earth 4.5 Gyr ago, these lunar semimajor axes are reached in less than 40 Myr. By comparison, the lunar sample 76535 shows evidence of a lunar magnetic field 4.2-4.3 Gyr ago (Garrick-Bethell et al. 2009).

Requiring the core to be decoupled from the mantle at that time allows us to place a lower limit on the average rate of tidal evolution during this epoch. The rate of tidal evolution is no slower than a factor of about 6 compared to the average tidal evolution rate. For the constant Δt Mignard model this implies $\Delta t > 0.44$ minutes, compared to today's value of about 10 minutes.

The Cassini transition occurs at around $33.4R_e$. We see that it is likely that the core did not follow the mantle during the Cassini transition. Since the obliquity of the Moon is large during the Cassini transition, we may speculate that there was a large magnetic field during the transition because of the large stirring (presuming the hypothesis of Dwyer and Stevenson, 2005). So we might expect nonzero lunar paleomagnetic measurements to cluster near the time of the Cassini transition, perhaps allowing us to constrain that time. At present there are not enough paleomagnetic data to assess this hypothesis.

3. Conclusion

The fluid core of the Moon does not precess with the mantle of the Moon. We have shown that this is also the case for much of lunar history. But when the Moon was close to the Earth the core followed the mantle. The transition occurred at $26.0R_e$ - $29.0R_e$.

Dwyer and Stevenson (2005) suggested that the lunar dynamo needs mechanical stirring to power it. The stirring is caused by the lack of locked precession of the lunar core. So, we do not expect a lunar dynamo powered by mechanical stirring when the Moon was close to the Earth.

4. Appendix

We consider here a simple model that illustrates and illuminates the transition from locked to unlocked core. Our model system is a core-mantle system perturbed by a third body. We assume the orbital period is short enough compared to the natural periods of the core-mantle system that the potential interaction can be averaged over the orbit. We assume the orbit is fixed and circular, with zero inclination to the ecliptic. For the real Moon the orbit is slightly inclined and regresses with an 18.6 year period, and the regression of the mantle of the Moon is locked to the regression of the orbit. In this simple model the mantle regresses uniformly at a rate determined by its obliquity and moments.

Following Touma and Wisdom (2001), we describe the core-mantle system, with zero amplitude wobble, by the Hamiltonian

$$H_{CM}(t, \theta, \Theta) = \omega_c \Theta + \frac{1}{2} k \Theta^2, \tag{15}$$

where, as before,

$$\omega_c = f_c \omega \frac{C}{C_m} \tag{16}$$

is the precession frequency of the core tilt mode, f_c is the core flattening, ω is the rotational angular frequency, C is the principal moment of the body, and C_m is the principal moment of the mantle. The nonlinearity parameter is

$$k = -\frac{f_c}{\delta C} \left[\frac{1 - 2\delta^2 + \delta^3}{(1 - \delta)^3} \right], \tag{17}$$

where $\delta = C_c/C$, where C_c is the principal moment of the core. Note that the nonlinearity parameter is large for both small and large core. Let g' be the angle that measures the direction of the tilted core in inertial space. The canonical coordinate $\theta = -g'$. The canonical momentum Θ is a measure of the tilt J of the symmetry axis of the core-mantle boundary from the angular momentum of the body. We have

$$\sin^2 J = \frac{2G'}{C\omega}, \tag{18}$$

with

$$G' = (c^2/D)\Theta, \tag{19}$$

where $c = -\sqrt{\delta}$ and $D = 1 - c^2$. The tilt K of the core rotation axis from the symmetry axis of the body is approximately $K = J/\delta$. See Touma and Wisdom (2001) for more details.

Again following Touma and Wisdom (2001), the potential energy is

$$n^2(C - A)P_2(\cos\theta_s), \tag{20}$$

where n is the mean orbital motion, C and A are the largest and smallest principal moments of the core-mantle body, and θ_s is the angle from the symmetry axis of the mantle to the perturbing body. The complete expression for the potential can be found in Touma and Wisdom (2001). Averaging over the orbital period is straightforward and simpler than the analysis in Touma and Wisdom (2001) because we are taking the orbit to be circular. The resulting averaged potential energy is

$$\begin{aligned} n^2(C - A) \Bigg[&-\frac{1}{2} + \frac{3}{8}\cos^2 I \sin^2 J + \frac{3}{4}\cos^2 J \sin^2 I + \frac{3}{8}\sin^2 J \\ &+ \frac{3}{2}\cos I \cos J \sin I \sin J \cos(f' - g') - \frac{3}{8}\sin^2 I \sin^2 J \cos(2f' - 2g') \Bigg], \end{aligned} \tag{21}$$

where I is the obliquity of the symmetry axis of the body to inertial z-axis (which is perpendicular to the fixed orbit plane), and f' is the angle of the ascending node of the equator on the orbit plane. The precession of the body is largely independent of the core mode dynamics, so we take the obliquity to be fixed, and $f' = -\omega_f t$, where the rate of regression of the equator is

$$\omega_f = \frac{3}{2}\frac{n^2(C - A)}{C\omega}\cos I. \tag{22}$$

The fact that the angles only appear in the combination $f' - g'$ and that f' is uniformly regressing suggests a transformation to a rotating frame. We choose a new coordinate $\theta' = f' - g' = \theta - \omega_f t$ with canonical momentum $\Theta' = \Theta$. Finally, we use the non-singular canonical variables

$$y = \sqrt{2\Theta'}\sin\theta' \tag{23}$$

$$x = \sqrt{2\Theta'}\cos\theta'. \tag{24}$$

The Hamiltonian is

$$\begin{aligned} H(t,y,x) &= (\omega_c - \omega_f)\frac{x^2+y^2}{2} + \frac{1}{2}k\left(\frac{x^2+y^2}{2}\right)^2 + \\ &\quad + n^2(C-A)\left[\frac{3}{2}(\cos I \sin I)\alpha x + \right. \\ &\quad + \left(\frac{3}{4} - \frac{9}{8}\cos^2 I\right)\alpha^2(x^2+y^2) - \frac{3}{8}(\sin^2 I)\alpha^2(x^2-y^2) \\ &\quad \left. -\frac{3}{4}(\cos I \sin I)\alpha^3 x(x^2+y^2)\right] \end{aligned} \tag{25}$$

where $\alpha = \sqrt{\delta/((1-\delta)C\omega)}$, and we have left out some constant terms. Note that we used the approximation $\cos J = 1 - (\sin^2 J)/2$, as J is small. Note that though J remains small, K can be large.

We carried out a numerical experiment to track the fixed points of the system as we varied the core flattening. We used parameters for the Moon, as given in the body of the text. We integrated the equations of motion with the Bulirsch-Stoer algorithm. We added a small dissipation so that the system would settle on the fixed points. We started the integrations with initial conditions for x and y very close to zero. Figure 3 shows the magnitude of K for the resulting fixed points as a function of the core flattening. We see that for large flattening the offset of the core to the mantle symmetry axis goes to zero. For ω_c near ω_f the system passes though a resonance and there is large offset of the core to the mantle. Then for small core flattening the core is offset from the mantle by the obliquity $K = I$.

The pattern of bifurcations and fixed points on the phase portraits (the trajectories in the $x - y$ plane) are those of a first order resonance. We can obtain the standard approximate Hamiltonian for a first order resonance by keeping only the first three terms in the

Hamiltonian. The resonance is between the precession of the core and the precession of the equator. We obtain

$$H(t,y,x) = (\omega_c - \omega_f)\left(\frac{x^2+y^2}{2}\right) + \frac{1}{2}k\left(\frac{x^2+y^2}{2}\right)^2 + n^2(C-A)\frac{3}{2}(\cos I \sin I)\alpha x \quad (26)$$

Using this approximate Hamiltonian we can derive the limiting values of the fixed points for small and large core flattening. The fixed points are on the $y = 0$ axis, and satisfy

$$0 = \frac{\partial H}{\partial x} = (\omega_c - \omega_f)x + \frac{1}{2}kx^3 + n^2(C-A)\frac{3}{2}(\cos I \sin I)\alpha. \quad (27)$$

Away from resonance we can ignore the nonlinearity term (i.e. set $k = 0$), and find the fixed points to be

$$x = -\frac{n^2(C-A)\frac{3}{2}(\cos I \sin I)\alpha}{\omega_c - \omega_f}. \quad (28)$$

For small flattening, $\omega_c << \omega_f$ and we find

$$\sin K = \sin I, \quad (29)$$

exactly. So the core spin axis is offset from the mantle symmetry axis by the obliquity, and thus is normal to the orbit plane. In the other limit of large flattening, $\omega_c >> \omega_f$, and therefore the fixed point approaches zero.

5. Acknowledgments

We thank Stan Peale for a helpful review and for drawing the connection that a stirring-powered dynamo might have been strongest during the Cassini transition. We also thank Dave Stevenson, Ben Weiss, and Jim Williams for helpful conversations.

REFERENCES

Dickey, J., Bender, P.L., Faller, J.E., Newhall, X.X., Ricklets, R.L., Riess, J.G., Shelus, P.J., Veillet, C., Whipple, A.L., Wiant, J.R., Williams, J.G., and Yoder, C.F. 1994, Lunar Laser Ranging: A Continuing Legacy of the Apollo Program, *Science*, **265**, 482.

Dwyer, C.A. and Stevenson, D.J. 2005, An Early Nutation-Driven Lunar Dynamo, *AGU Fall Meeting Abstracts* GP42A-06.

Garrick-Bethell, I., Wisdom, J., and Zuber, M. 2006, Evidence for a Past High Eccentricity Lunar Orbit, *Science* **313**, 652.

Garrick-Bethell, I., Weiss, B.P., Shuster, D.L., and Buz, J. 2009, Early Lunar Magnetism, *Science* **323**, 356.

Goldreich, P. 1967, Precession of the Moon's Core, *JGR* **72**, 3135.

Kuskov, O.L. and Kronrod, V.A. 1998, Constitution of the Moon, *PEPI* **107**, 285.

Meyer, J. and Wisdom, J. 2010, Coupled Thermal-Orbital Evolution of the Early Moon, *Icarus*, **208**, 1-10.

Peale, S.J. 1968, Generalized Cassini's Laws, *Astron. J.* **74**, 483.

Poincaré, H. 1910, Sur la précession des corps déformables, *Bulletin Astronomique, Serie I* **27**, 321.

Toomre, A. 1966, On the Coupling of the Earth's Core and Mantle during the 26,000-Year Precession, in *The Earth-Moon System*, eds. Marsden, B.G. and Cameron, A.G.W., (Plenum Press, 1966), 33.

Touma, J. and Wisdom, J. 1994, Evolution of the Earth-Moon System, *Astron. J.* **108**, 1943.

Touma, J. and Wisdom, J. 2001, Nonlinear Core-Mantle Coupling, *Astron. J.* **122**, 1030.

Ward, W.R. 1975, Past Orientation of the Lunar Spin Axis, *Science* **189**, 377.

Williams, J.G., Boggs, D.H., Ratcliff, J.T. 2009. A Larger Lunar Core? *Lunar and Planetary Institute Science Conference Abstracts* **40**, 1452.

Wisdom, J. 2006, Dynamics of the Lunar Spin Axis, *Astron. J.* **131**, 1864.

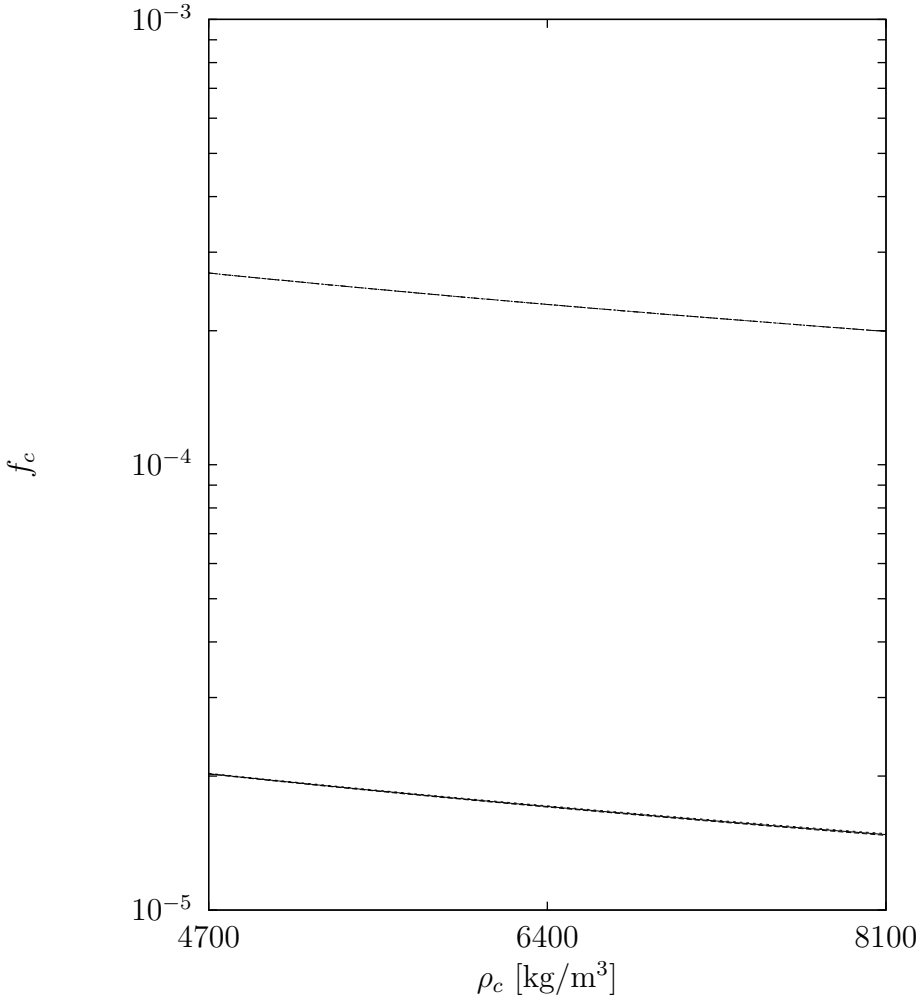

Fig. 1.— The flattening of the lunar core plotted versus the assumed density of the core, for fixed core moment of inertia. For the non-hydrostatic mantle model, three curves are plotted. These three curves are the upper three on the plot and indistinguishable from each other. These three curves correspond to different core moments: $C_f/C = 0.8 \times 10^{-3}$, 1.2×10^{-3} and 1.6×10^{-3}. Similarly, the lower curves (also indistinguishable) show the results for the hydrostatic mantle model and the same core moment values.

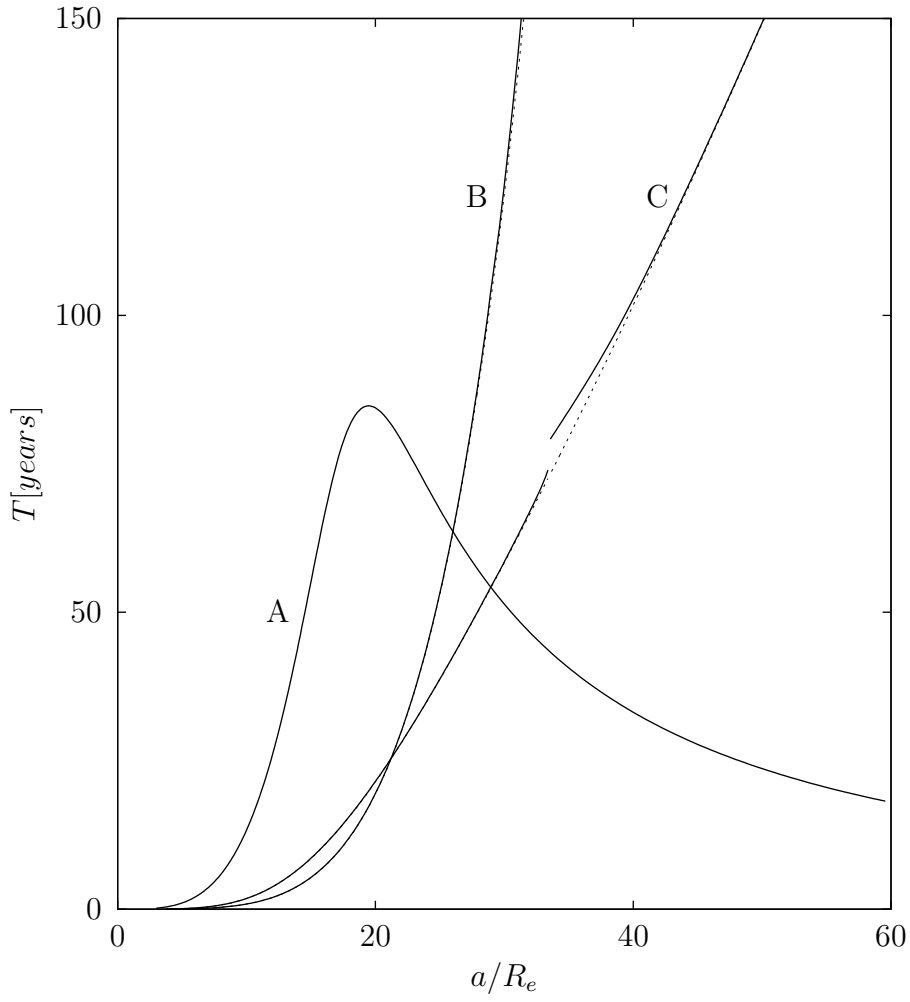

Fig. 2.— The period of precession of the lunar orbit and lunar mantle (line A), of the lunar core in the "hydrostatic mantle" model (lines B), and of the lunar core in the "non-hydrostatic mantle" model (lines C), plotted as a function of lunar semimajor axis in Earth radii. For lines B and C the solid line takes into account the forced obliquity of the Moon, whereas the dashed line assumes zero obliquity. The gap in the non-hydrostatic mantle model occurs at the Cassini transition. The core precesses with the mantle when the Moon is close to the Earth; and the lunar core decouples from the mantle at large semimajor axis. The point of transition depends on the model.

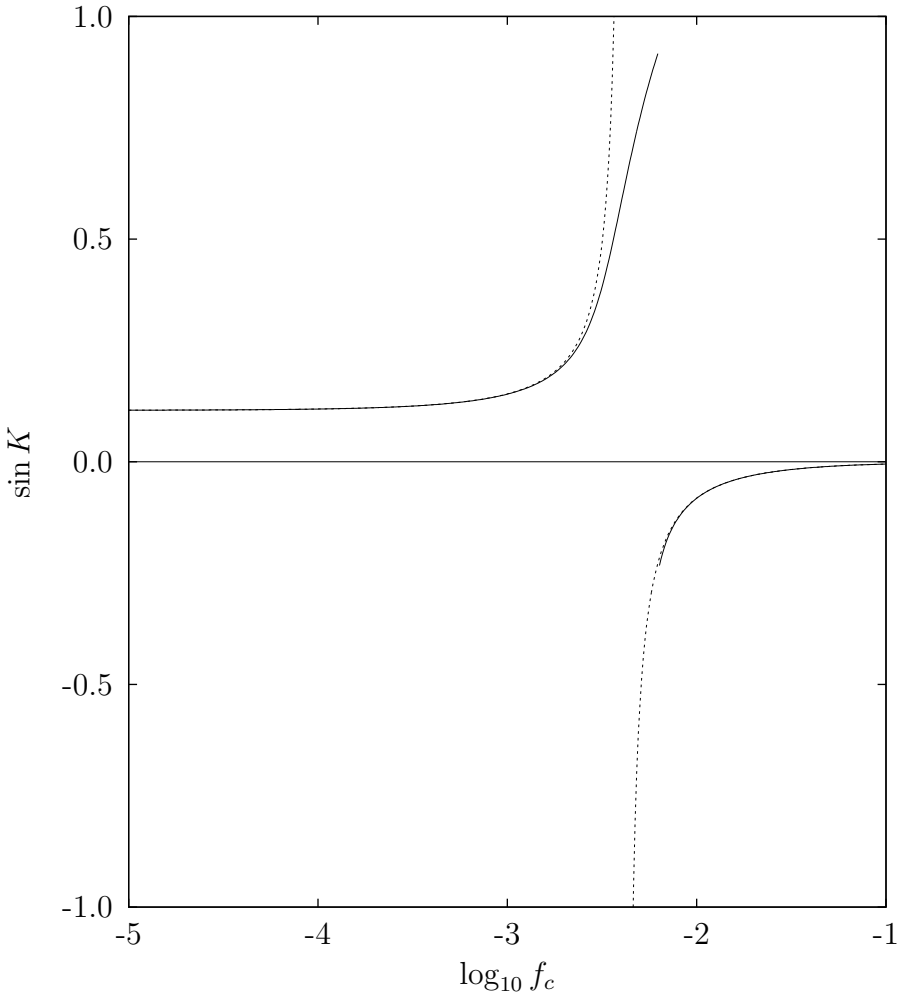

Fig. 3.— The offset of the core spin axis from the mantle symmetry axis is plotted versus the core flattening for the equilibrium points of the system. The equilibrium points are found by adding a small dissipation and integrating the equations of motion. Two broken curves are shown. For the solid curve the full resonance Hamiltonian was used; for the dotted curve the nonlinearity parameter k was set to zero. For small flattening the offset of the core is approximately the obliquity; the core spin axis is perpendicular to the orbit. For large flattening, the offset tends to zero; the core spin axis is locked to the mantle.